Polymorphism in Self-Assembled Terphenylthiolate Monolayers on Au(111)

ARTICLE *in* LANGMUIR · OCTOBER 2013

Impact Factor: 4.46 · DOI: 10.1021/la403116r · Source: PubMed

4 AUTHORS, INCLUDING:

Asif Bashir
Max Planck Institute for Iron Research GmbH
50 PUBLICATIONS **552** CITATIONS
SEE PROFILE

Waleed Azzam
Tafila Technical University
26 PUBLICATIONS **923** CITATIONS
SEE PROFILE

Langmuir

Article

pubs.acs.org/Langmuir

Polymorphism in Self-Assembled Terphenylthiolate Monolayers on Au(111)

Asif Bashir,*[,§] Waleed Azzam,[†,‡] Michael Rohwerder,[§] and Andreas Terfort*[,#]

[§]Max-Planck-Institut für Eisenforschung GmbH, Max-Planck-Straße 1, 40237 Düsseldorf, Germany

[†]Department of Chemistry, Tafila Technical University, P.O. Box 179, 66110 Tafila, Jordan

[‡]Department of Chemistry, University College in Al-Qunfudah, Umm Al-Qura University, 1109 Makkah Al-Mukarramah, Saudi Arabia

[#]Institute of Inorganic and Analytical Chemistry, Goethe-University, D-60438 Frankfurt, Germany

ABSTRACT: Self-assembled monolayers (SAMs) of terphenylthiol (TPT) on gold Au(111) substrates exhibit well-ordered structures over large scales if they are annealed in ethanol at 40 °C after their formation. Using high-resolution STM, two distinct, ordered phases could be observed. The simpler phase, designated as α-phase, consists of closely packed molecules in the well-known $(2\sqrt{3} \times \sqrt{3})R30°$ structure. It could be demonstrated that under less suitable imaging conditions this phase can be mistaken as the hexagonal $(\sqrt{3} \times \sqrt{3})R30°$, which resolves a discrepancy in between previous reports. The second phase is characterized by a stripe pattern with a periodicity of 2.0 nm and can be described by a point-on-line incommensurate $(4 \times n)$ ($\begin{bmatrix} 4 & 0 \\ 0 & n \end{bmatrix}$) lattice with n close to 8. This β-phase contains four pairs of terphenylthiolate molecules, which might be held together by either disulfide bonds or the recently discussed S−Au−S motif, and is thus 35% ± 15% less densely packed than the α-phase. The coexistence of these phases explains the variability of spectroscopic results obtained in the past for terphenylthiolate layers, since their relative proportion determines the average thicknesses/tilt angles found in these studies.

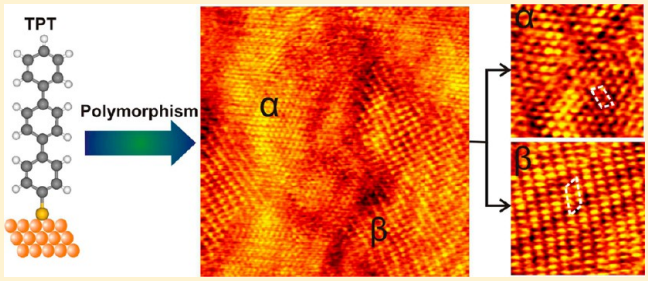

1. INTRODUCTION

The formation of stable, well-ordered, and densely packed self-assembled monolayers (SAMs) on solid surfaces has become the focus of broad academic interest.[1−5] The wide attention attracted by SAMs is due to the large diversity of existing and potential applications in a variety of fields such as antifouling,[6,7] biosensorics,[8−10] electrochemistry,[11,12] and lithography.[13−16] Still, the majority of SAM studies are performed on alkanethiol-based SAMs on Au(111), which can be easily prepared by immersion of the substrates into solutions of the corresponding thiol.[1,2] Recently, SAMs of conjugated molecules became very popular due to their potential applications in molecular electronics[17,18] and electronic interfaces.[19,20] In previous studies, it has been found that the precise structural arrangement within the SAMs of conjugated aromatic thiolates depends critically on a complicated balance of contributions such as intermolecular interactions and anchor−substrate bonding.[21−24] The rational design of such monolayers requires specific knowledge of these factors and their relative importance. Therefore, several studies have been carried out to understand the structure and kinetics of film formation of conjugated aromatic thiols on gold surfaces.[24−30] Since biphenyl (BP) and terphenyl (TP) based thiolate SAMs are representative of conjugated SAMs, the high coverage phases of these SAMs have been examined in considerable detail using various spectroscopic and microscopic techniques.[10,15,25−27,31−44] Just recently, two groups independently reported on the structure of the monolayers of the unsubstituted biphenylthiol (BPT).[38,39] Kang et al. reported the formation of a well-ordered $(\sqrt{3} \times \sqrt{3})R30°$ structure on Au(111) from ethanol at 60 °C after short deposition times.[38] This structure was overlaid by a stripe pattern with a distance of 2.0−3.5 nm formed by linear assemblies of small clusters (about 1 nm in diameter) with five to six differently bound BPT molecules each. The authors reported that the structural order of these films decreases with increasing immersion time.[38] On the other hand, Turchanin et al. found that BPT SAMs on Au(111) formed either by vapor deposition or by wet chemistry using dimethylformamide (DMF) as solvent show a hexagonal (2×2) superstructure of almost upright oriented molecules.[39] Upon annealing, this structure turned into a mixture of less dense phases, such as the $(9 \times 3\sqrt{3})$, the $(8 \times 2\sqrt{3})$, or the $(2 \times 7\sqrt{3})$ phase. In contrast to BPT, terphenylthiol (TPT) has so far only reported to yield SAMs of fairly low structural quality and only very small ordered domains.[31−33] The order within these small domains was described as densely packed

Received: August 15, 2013
Revised: September 19, 2013
Published: October 1, 2013

   dx.doi.org/10.1021/la403116r | *Langmuir* 2013, 29, 13449−13456

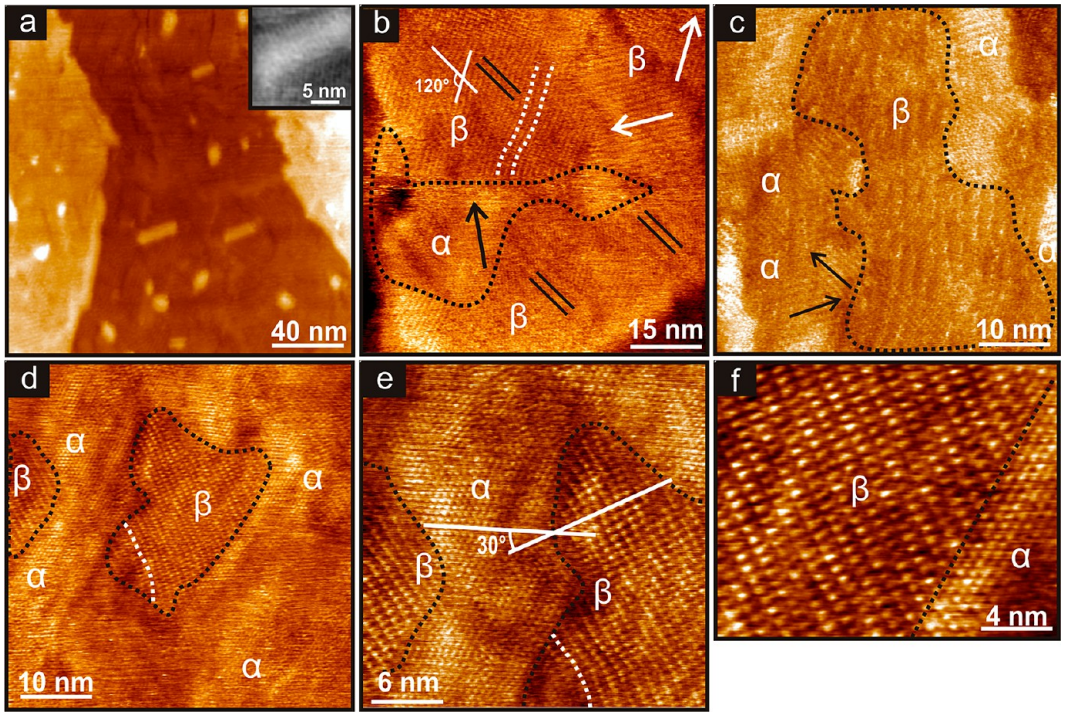

Figure 1. STM images of TPT monolayers on Au(111) taken at different resolutions. In a general overview (a), the Au monolayer islands are clearly visible. These islands are also covered by ordered monolayers (inset). At larger magnifications (b-f), the α-phases and β-phases become distinguishable. Domain boundaries are marked by black dashed lines. In b, the parallel black lines show the width of the stripes observed in the β-phase, while the dashed white curves signify the line faults occurring within the ordered domains of the β-phase. The white and black arrows show the main directions visible in the ordered domains of the α- and β-phase, respectively. The dashed white curves in d and e mark the same row of molecules within the β-phase domain, while the scan direction has been rotated to verify that the structures are not a scanning artifact. The intersecting white lines in e demonstrate that the α-and β-phases are rotated by 30° with respect to each other. The two phases contact each other without any area of disorder (f).

molecules with the molecular axes slightly tilted away from the surface normal forming a either a $(\sqrt{3} \times \sqrt{3})R30°$ or a $(2\sqrt{3} \times \sqrt{3})R30°$ superstructure.[31−33] Besides this dense phase, the Ishida group found several other phases, depending on the deposition conditions, one of them described as consisting of flat-lying molecules, but again with a very limited long-range order.[32,33]

In this paper, we wish to present that it is in fact possible to attain TPT SAMs with a long-range order comparable to alkanethiol SAMs. By careful optimization of the preparation conditions, the quality of TPT SAMs on Au(111) could be improved substantially, allowing to record high resolution STM images. These data, which show true molecular resolution, reveal the coexistence of two structural phases in TPT SAMs. In addition to the (expected) close packed $(2\sqrt{3} \times \sqrt{3})R30°$ phase a low density, striped phase was found. The new results also resolve a number of apparent inconsistencies between previously reported results.

2. EXPERIMENTAL SECTION

2.1. Preparation of Gold Substrates. STM measurements have been carried out on substrates that have been prepared by evaporating 140 nm of Au onto freshly cleaved mica, which has been heated to about 600 K for three days in the evaporation chamber. After evaporation of the metal, the substrates were cooled and the chamber was backfilled with nitrogen. The substrates were stored under argon and flame-annealed in a butane/oxygen flame immediately before the adsorption experiments were carried out. This procedure yields Au substrates with large terraces (several hundreds of nanometres, as evidenced by STM) exhibiting a (111) surface.

2.2. Chemicals. *p*-Terphenylthiol was synthesized using a previously described procedure.[44] Acetone, absolute ethanol (both Merck KGaA, Germany), and dichloromethane (CH_2Cl_2, Sigma-Aldrich) were used as received.

2.3. Preparation of SAMs. The formation of the TPT monolayers was carried out by immersing the substrates into 1 mM solutions of TPT in ethanol for 18 h at RT. Then the samples were gently annealed for 30 to 40 min in pure ethanol at 40 °C, before the samples were rinsed with ethanol, dichloromethane, acetone, and ethanol again. Each rinsing step took one to two minutes. The substrates then were dried in a stream of N_2.

2.4. Scanning Tunneling Microscopy (STM). All STM measurements were carried out in air, using a Jeol JSPM 4210 microscope which had been cross-calibrated by imaging HOPG with atomic resolution. The tips were prepared mechanically by cutting a 0.25 mm $Pt_{0.8}Ir_{0.2}$ wire (Goodfellow). All data were collected in constant-current mode with typical tunneling currents of 0.13−0.3 nA and a sample bias of 0.4−1.0 V.

3. RESULTS AND DISCUSSION

By adaption of a deposition/rinsing procedure reported for another aromatic thiol, anthracene thiol,[23] we found that films with good molecular order could be obtained, if the deposition step is followed by thorough rinsing with different solvents. Figure 1 shows representative STM data obtained for the TPT SAMs on Au(111). The image collected at large scale (Figure 1a) shows several terraces separated by steps with the height of an atomic Au(111) layer, 0.24 nm. This image also shows irregularly shaped islands not present on the clean Au(111) substrate before the SAM formation process. The height of these islands (0.24 nm) reveals that they correspond to a

dx.doi.org/10.1021/la403116r | *Langmuir* 2013, 29, 13449−13456

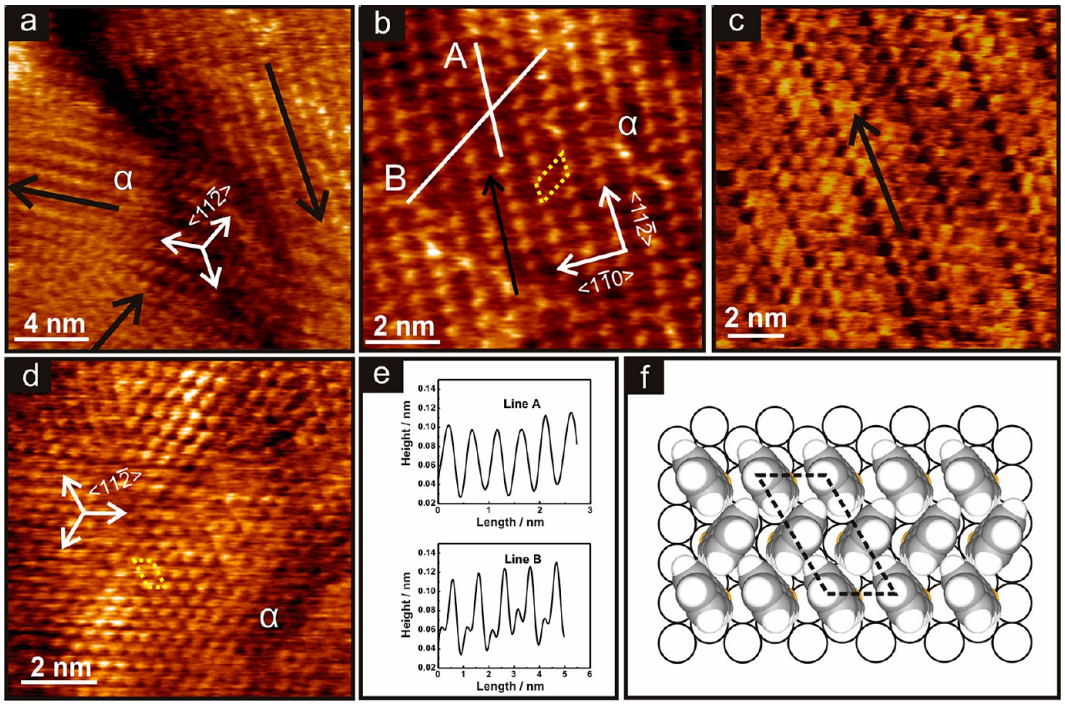

Figure 2. High-resolution STM images of the α-phase of the TPT monolayers (a-d). The black arrows show the main directions of the ordered domains, which run parallel to the $\langle 11\bar{2}\rangle$ directions of the Au(111) substrate. In a, three of these domains are visible with their main directions rotated by 120° with respect to each other. In b, the yellow, dashed box marks the $(2\sqrt{3} \times \sqrt{3})R30°$ oblique unit cell. The length of the unit cell vectors are 0.52 ± 0.03 nm and 1.03 ± 0.04 nm. The second set of molecules (along the black arrow) is invisible due to the tunneling conditions (I = 0.13 nA and sample bias 0.4 V; see main text). In c, the tunneling conditions (I = 0.2 nA, U = 0.4 V) make these molecules visible, but still double rows of molecules with a trench in between can be seen. The molecules become all (seemingly) equivalent upon reducing the impedance further (I = 0.4 nA, U = 0.4 V), so that the arrangement looks like the hexagonal $(\sqrt{3} \times \sqrt{3})R30°$ structure (d). The cross-sectional height profiles taken along the lines A and B in b permit the determination of the unit cell vectors. A model of the $(2\sqrt{3} \times \sqrt{3})R30°$ structure of the α-phase of TPT on Au(111) is shown in (f).

monolayer of Au atoms, which are also covered by the SAM (see inset in Figure 1a). The islands typically have diameters of 5−20 nm and are randomly distributed over the gold substrate. Note that the adsorption-induced formation of such islands is typical for molecules, in which the anchoring group (S or Se) is attached directly to the aromatic moiety (such as BPT,[39] biphenylselenol (BPSe),[45] anthraceneselenol (AntSe),[46] or phenylselenol (PSe)[21]), while for alkanethiolate SAMs on Au, normally vacancy pits resulting from the removal of Au atoms from the top Au(111) layer are observed.[3,47] When compared to the other aromatic SAMs, the islands formed by the adsorption of TPT are found to have smaller size and lower density than those observed for BPT, BPSe, and PSe films on Au. For BPT or BPSe systems,[39,45] the diameter of the islands was found to be 5−40 nm, and in the case of PSe,[21] the diameter was 30−40 nm.

Generally, these islands were attributed to gold atoms which have been expelled from the surface due to the lifting of the so-called "herring-bone" reconstruction, in which the Au atom density is increased by 4.2% compared to the non-reconstructed Au(111)-surface.[48] The question, why for most organothiols not these expected islands but pits are seen, is a subject of ongoing controversy.[49,50]

Figure 1b-f shows high (molecular) resolution data of the TPT films. The STM images shown in b and d-f were recorded in areas where the islands were absent. Closer inspection of these STM micrographs reveals the presence of two different structural phases, α and β, the borders between which are marked in the STM images by black dashed lines. The ordered domains of the α- and β-phases are typically 10−50 nm in diameter with an almost equal distribution. In contrast to the β-phase, the order in the α-phase could hardly be recognized at large scale images such as the one shown in Figure 1b. At this magnification, it can already be seen that the β-phase exposes striped structures with a separation of ∼2.0 nm (see the parallel black solid lines in b). These features show a 120° relationship between different domains due to the trigonal symmetry of the Au(111) surface (see the white arrows in b). Within a single domain, these stripes are often interrupted by line faults running almost perpendicular to the stripe direction (see the white dashed lines in Figure 1 b). This feature will be discussed in detail later.

At higher magnifications, molecular resolution can also be attained for the α-phase (Figure 1c-f). Again, a main direction of the structures can be seen, with a 120° relationship between different domains (black arrows in c). Nevertheless, the orientations in the α- and β-phase are not collinear, but are rotated by 30 ± 5° with respect to each other as indicated in Figure 1e, hinting on substantially different structures. Closer inspection of the STM images reveals another import difference between the α- and β-phase: As can be seen in Figure 1f, the shape and size of the spots along the TPT molecular rows of the ordered domains are different for the two phases. In the α-phase, these spots are smaller in size than the ones observed in the β-phase and adopt a spherical shape. In contrast, an elliptical shape was observed for the spots forming the β-phase. In addition, the distance between the neighboring spots is different for the two phases. These issues will be addressed in

dx.doi.org/10.1021/la403116r | Langmuir 2013, 29, 13449−13456

the following discussion of the structures of the α- and β-phases.

3.1. α-Phase. The details of the molecular structure formed by the TPT species within the α-phase can be deduced from the high-resolution STM images shown in Figure 2. As can be seen in Figure 2a, the orientation of the different domains is correlated by 120° (black arrows), with the main direction being in line with the $\langle 11\bar{2}\rangle$ direction of the substrate. The appearance of the molecular pattern was found to depend significantly on the tunneling conditions. When a large tunneling impedance of ~3 GΩ (tunneling current I = 0.13 nA and a sample bias U = 0.4 V, resulting in a large tip−sample distance, Figure 2b) was used, clearly two nonequivalent directions can be distinguished, which run parallel to the $\langle 11\bar{2}\rangle$ and the $\langle 1\bar{1}0\rangle$ substrate directions, respectively. The dark rows defining the main direction of the structure become even more pronounced for moderate tunneling impedances, for instance ~2 GΩ (I = 0.2 nA and U = 0.4 V, Figure 2c). Surprisingly, at small tunneling impedances such as ~1 GΩ (I = 0.4 nA and U = 0.4 V, Figure 2d), the dark rows disappear and a hexagonal surface structure was observed.

The dimensions of the 2D unit cell of the α-phase were determined from the height profiles along the molecular rows (e.g., along the lines A and B in Figure 2b). For line A, a periodic pattern with no extra features and a periodicity of a = 0.52 ± 0.03 nm was found, while along line B a repeating pattern with two inequivalent maxima and a periodicity of b = 1.03 ± 0.04 nm can be observed (Figure 2e). The second maximum indicates the presence of a second molecular row (darker row) in between the brighter rows along the $\langle 11\bar{2}\rangle$ direction. With these observations taken together, it can be concluded that the unit cell corresponds to a $(2\sqrt{3} \times \sqrt{3})R30°$ structure ($\begin{bmatrix} 2 & \bar{2} \\ 2 & 1 \end{bmatrix}$ structure in the matrix notation) with two molecules per unit cell, a structure often observed for alkanethiolate-based SAMs, but which has also been seen in a number of organothiolate SAMs comprising aromatic moieties.[24−28] The data are consistent with the sulfur atoms positioned on a $(\sqrt{3} \times \sqrt{3})R30°$ lattice and the unit-cell containing two inequivalent molecules, what often is explained by a different twist angle (with respect to the substrate) of the two kinds of molecules resulting in different electronic coupling efficiencies between the tip and the substrate.[26,31] This herringbone-like arrangement of the TPT molecules is displayed in the structural model for the $(2\sqrt{3} \times \sqrt{3})R30°$ phase in Figure 2f. In this structure, the area occupied by a single TPT molecule amounts to 0.216 nm^2. The tilt-angle θ for the terphenyl backbone within the α-phase can thus be estimated by considering the van der Waals dimensions of the phenyl rings, 0.64 nm × 0.33 nm,[31] yielding a cross-sectional area of 0.211 nm^2. Using a simple calculation (θ = arcos(0.211 nm^2/0.216 nm^2)) then yields a terphenyl-backbone tilt angle of 13° with respect to the surface normal.

It is worth mentioning that the $(2\sqrt{3} \times \sqrt{3})R30°$ structure has been assigned to the TPT monolayers on Au(111) earlier,[31] but so has been the $(\sqrt{3} \times \sqrt{3})R30°$ structure.[32,33] Since the packing density of both phases is the same, typical spectroscopic methods, such as infrared reflection absorption spectroscopy (IRRAS) or near-edge X-ray adsorption fine structure (NEXAFS) spectroscopy cannot distinguish between these phases. We assume that the assignment to the higher-symmetry $(\sqrt{3} \times \sqrt{3})R30°$ structure was due to the choice of unsuitable STM conditions, presumably too low impedance, as we could demonstrate above. It has been known that the origin of contrast formation in STM depends strongly on the tunneling gap impedance what may lead to the assignment of a wrong unit cell.[51] Our results therefore allow to resolve the apparent discrepancies between previous studies concerning the structure of TPT SAMs on Au(111).

3.2. β-Phase. As mentioned above, the β-phase shows two striking differences to the α-phase, namely, a different shape of spots and the presence of parallel stripes with a distance of approximately 2 nm. While these are quite faint in large area STM images, such as the one in Figure 1b, they become clearly visible at larger magnifications such as those shown in Figure 3a and b. At intermediate magnifications a second set of finer lines can be distinguished, which run almost perpendicular to the previous ones. These lines do not run straight through the domains but become curved/distorted in the vicinity of the α-phases (see white dotted lines in Figure 1b, d, and e). In order to exclude a possible influence of the scanning tip on the straightness of the rows, the image shown in Figure 1e was recorded after zooming into a region shown in the center of the image d while changing the direction of the scan (scan angle). Almost the same bend was observed for the same row of molecules (see the white dotted line in e). The formation of these bends along the molecular rows can be explained by the presence of several translational domain boundaries (line faults) within the ordered domains of the β-phase as can be seen in Figure 3a and b. In these images, the neighboring translational domain boundaries are marked by white dotted lines to guide the eyes of the reader. The distance between the line faults is typically about 5−8 nm. Such a high density of

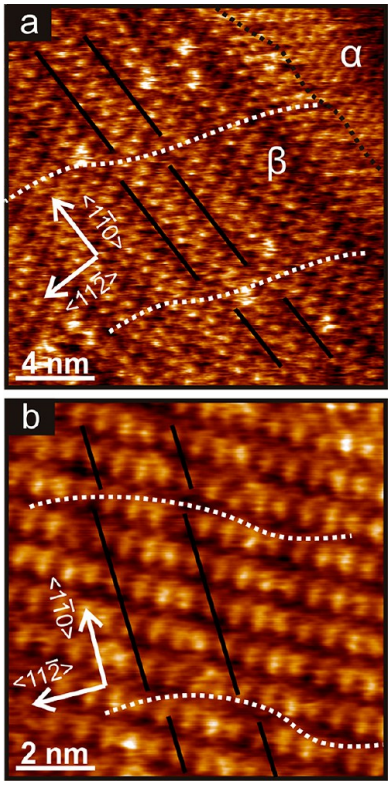

Figure 3. High-resolution STM images of the β-phase in which the fault lines become visible (white dashed lines). The translational domains are visualized by the parallel black lines which guide the eye for the "dark row" feature in the β-phase.

dx.doi.org/10.1021/la403116r | Langmuir 2013, 29, 13449−13456

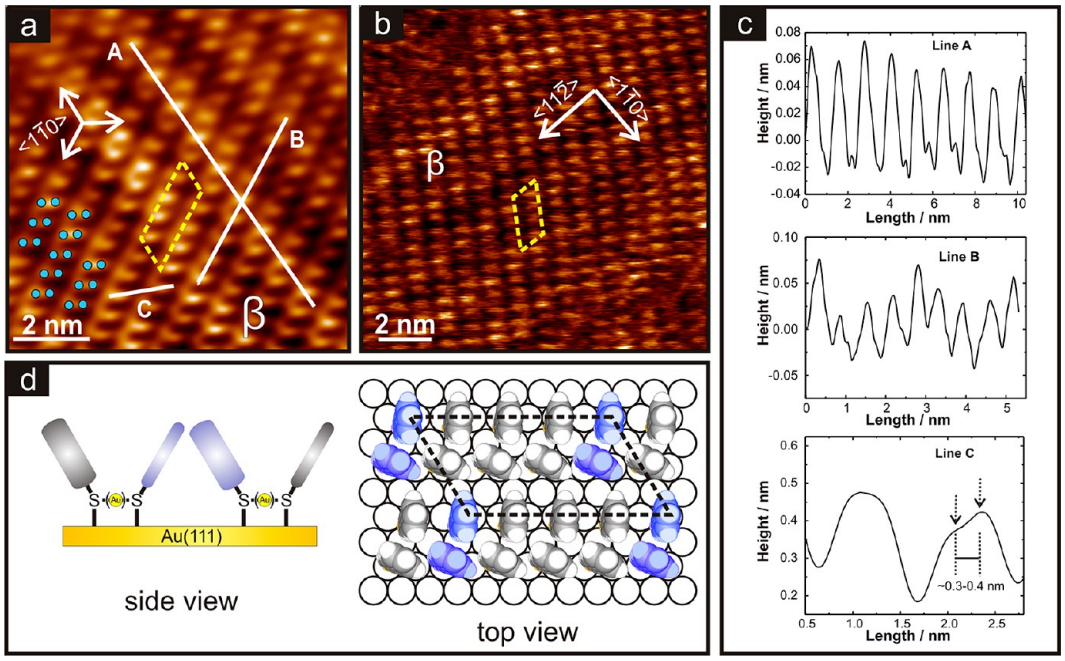

Figure 4. High-resolution STM images of single domains of the β-phase (a and b). The yellow, dashed boxes mark the $(4 \times n)$ unit cell with n close to 8. Its average size is $a = 1.2 \pm 0.08$ nm and $b = 2.4 \pm 0.05$ nm with an angle of $120 \pm 5°$. These values were determined from the cross-sectional height profiles (c) taken along the lines A and B in b. Profile C demonstrates that each oval spot consists of two maxima (depicted as blue circles in a), leading to the model of the β-phase of TPT on Au(111) shown in d (depicted is $n \sim 7.5$). The pair of molecules forming one oval spot is colored in blue. In the side view (left), the Au atoms are in parentheses because we cannot distinguish yet whether the pairs are held together by S−S bonds or by the recently devised S−Au−S 'handle' motif.

translational domains has been previously observed for conjugated, purely aromatic thiol SAMs, like anthracene thiol SAMs, and has been explained by the large misfit between the preferred lattice of the aromatic moieties and the Au(111) substrate lattice.[21,23,52,53] The translational boundaries seem to result from single steps along one of the two $\langle 1\bar{1}0 \rangle$ directions, which run 120° to the $\langle 1\bar{1}0 \rangle$ direction defining the main pattern (black solid lines). The curviness of these fault lines thus can be explained by a frequent change of direction along these two equivalent directions.

Within the domains, the high quality of the STM data allowed determining precisely the TPT molecular arrangement within the β-phase. Following the scan lines A and B in the high-resolution micrograph of a fault-line free domain (Figure 4a), the lattice vectors of the unit cell could be determined as $a = 1.2 \pm 0.08$ nm and $b = 2.4 \pm 0.05$ nm. Since these scan lines run along the $\langle 1\bar{1}0 \rangle$ directions, this would suggest the existence of a commensurate (4×8) cell, which would contain four of the oval spots. On a perfect Au(111) surface, such a cell should be equivalent to the smaller (4×2) cell containing only one oval spot. Nevertheless, the presence of the superstructure discussed earlier rather suggests a point-on-line incommensurability, so we need to formulate the cell as $(4 \times n)$ (in matrix notation $\begin{bmatrix} 4 & 0 \\ 0 & n \end{bmatrix}$) with n being close to 8. The variability in n would also explain the variability observed in the distance between the superstructure lines (2.0 ± 0.15 nm, black lines in Figures 1b and 3a and b).

As mentioned above, the spots along the molecular rows within the β-phase appear to be larger than those observed for the α-phase. A closer inspection of high-resolution data reveals that in fact each spot is composed of two overlapping spherical spots, with a distance of 0.25−0.4 nm. In many cases, the two overlapping spherical spots could be resolved in the cross-sectional height profile along line C (see Figure 4c). With two molecules per spot, a total of eight TPT molecules must be present per unit cell. When $n = 8$ is assumed for the unit cell, an area/molecule ratio of 0.288 nm^2 can be calculated. Using extremes such as $n = 7$ or $n = 9$, the respective molecular area would be 0.251 nm^2 and 0.323 nm^2, respectively. Applying the formula given above, these values result in tilt angles of 33−49° with respect to the surface normal. Such large tilt angles result in an effective decrease of the film thickness in the areas of the β-phase, which should be visible in the topography of the surface. Nevertheless, since the conduction path of the charge carriers typically is along the molecular axes, the length of which remains unchanged, only small 'apparent height' effects can be expected.

These large tilt angles also explain the observation of the ovals, since obviously the terphenyl units tilt toward each other in a pairwise manner, forming the observed elongated spots (see Figure 4d). We suggest that this tilting is caused by the proximity of the anchoring groups of the TPT molecules of two neighboring rows (see Figure 4d). This proximity might be caused by the formation of S−S (disulfide) bonds at the surface, what also has been postulated for SAMs formed from decanethiol,[54,55] 4-mercaptopyridine,[56,57] and 4-methylbenzenethiol[58] SAMs on Au(111). An alternative model would involve the formation of S−Au−S bonds by extrusion of Au atoms, a binding principle recently found for thiolates on Au nanoparticles and suggested as a general binding motif for SAMs.[59,60] Indeed, this binding mode has been observed in low-coverage layers of methanethiolate on Au(111) leading to stripes formed by CH_3S−Au−SCH_3 'pairs' with an Au atom that could be visualized by STM.[50] Since the TPT molecules used in this study are much larger than the methanethiolate

dx.doi.org/10.1021/la403116r | *Langmuir* 2013, 29, 13449−13456

ligands, we cannot expect to see the respective Au atoms, so we cannot distinguish between these two pairing schemes. In this context it is worth mentioning that − in contrast to the case of the α-phase − no particular influence of the imagining conditions on the pattern obtained for the β-phase could be observed. The reason for this presumably is that the two inequivalent TPT molecules in any case merge to the oval spots so that slight differences upon changing the gap impedancy become smeared out.

TPT phases with relatively large distances already have been observed by Ishida et al. in 2001.[33] These authors reported phases called β (deposited from dichloromethane) and ε (deposited from ethanol) with molecular lattices of $a = 0.65 \pm 0.05$ nm and $b = 1.25 \pm 0.04$ nm, which also showed oval spots. In fact, when doubling the cell vectors reported by these authors, the cell found in our study becomes almost reproduced. An important difference between the cells is their orientation: In ref 33 a $\begin{bmatrix} 5 & \bar{1} \\ \bar{1} & 3 \end{bmatrix}$ superstructure is suggested (only depicted), which is canted by 14° with respect to the nearest $\langle 1\bar{1}0 \rangle$ vector. This would result in a 44° or 16° relationship between this superstructure and the $(2\sqrt{3} \times \sqrt{3})R30°$ ($\begin{bmatrix} 2 & 2 \\ 2 & \bar{1} \end{bmatrix}$) superstructure of the α-phase. Since in our case, the angle between the two phases clearly can be determined as 30° ± 5° (Figure 1e), the $(4 \times n)$ ($\begin{bmatrix} 4 & 0 \\ 0 & n \end{bmatrix}$) superstructure is the more likely one. Furthermore, due to the technological limitations at that time, the oval spots in the cells could not be resolved and were assumed to be formed by flat lying molecules.[33] Thus, the identification of two molecules in each spot results in much smaller tilt angles, making the microscopic results more compatible with the spectroscopic results (see below). The use of advanced microscopy methods in combination with improved preparation procedures therefore made the correct assignment of the observed pattern possible.

Comparison with Spectroscopic Results. Since spectroscopic methods typically integrate over a larger surface area, the results for polymorphous monolayers depend not only on the properties of the individual phases, but also on their ratio. This is particularly relevant for the methods determining film thicknesses or molecular tilt angles, two values that are intertwined for densely packed films. For the TPT monolayers on gold, several studies have reported film thicknesses between 1.1 and 2.2 nm using either ellipsometry[42] or photoelectron spectroscopy.[31,43] With a molecular length of about 1.7 nm, and an estimated Au−S distance of about 0.2 nm, this corresponds to tilt angles of 0−54°. A study using a derivative of TPT, 4″-methylterphenylthiol, found a thickness of 1.7 nm and deduced a tilt angle of 17° ± 8° from this.[40] More exact values for the average tilt angles have been obtained by NEXAFS spectroscopy. In three studies, values of 20°,[43] 27° ± 5°,[44] and 28°[31] were found. While the deviation between these values can be explained by the typical error of the NEXAFS method, it may also be explained by different ratios between the α- and β-phase in the different samples. Depending on the exact ratio, average tilt angles between 13° (pure α-phase) and ∼41° (pure β-phase) can be expected. Since the α- and β-phase are present in almost equal amounts, as stated above, average angles of 23−31° should be found, what goes well in line with the values observed by the three NEXAFS studies. Thus, the current findings can easily explain the apparent deviation between the determined tilt angles and the orientation of the molecules expected in a pure $(2\sqrt{3} \times \sqrt{3})R30°$ phase.

4. CONCLUSIONS

In this work, the use of high-resolution STM in combination with an improved monolayer preparation procedure (involving annealing at 40 °C) permitted the determination of the polymorphism within the monolayers of terphenylthiol on gold(111) surfaces. Although this monolayer system has been studied since more than 20 years, the apparent discrepancies between the different studies could not be explained until now. Here, these issues could be resolved by finding the coexistence of two distinct phases, designated as α and β. While in the past, two structures, the $(\sqrt{3} \times \sqrt{3})R30°$ and the $(2\sqrt{3} \times \sqrt{3})R30°$ structure, have been assigned to the α-phase, we could clearly demonstrate that the appearance of the hexagonal phase is an imaging artifact because of suboptimal imaging conditions. Due to the dense packing in the $(2\sqrt{3} \times \sqrt{3})R30°$ ($\begin{bmatrix} 2 & 2 \\ 2 & \bar{1} \end{bmatrix}$) cell, the molecules stand almost upright (13° tilt with respect to the surface normal). The second phase, denominated β, is described by an oblique unit cell of which only one vector is fully commensurate with the gold lattice. The second vector has to be described by a point-on-line incommensurability due to the appearance of a periodic superstructure. We assign this cell as $(4 \times n)$ ($\begin{bmatrix} 4 & 0 \\ 0 & n \end{bmatrix}$) with n close to 8. The TPT moieties in this cell form pairs which become visible as ellipsoids in the STM images. With a total of eight molecules per unit cell, the packing in this phase is about 33% (for $n = 8$) less dense than in the α-phase, corresponding to an increased tilt angle of the terphenyl units (33−49°, depending on n).

The coexistence of these two phases explains the differences between the results of several previous studies, in which a variety of film thicknesses and molecular tilt angles have been reported. Since most spectroscopic methods integrate over larger areas, the relative ratio between the α- and β-phase results in different average thicknesses and tilt angles.

AUTHOR INFORMATION

Corresponding Author

*E-mail aterfort@chemie.uni-frankfurt.de.

Notes

The authors declare no competing financial interest.

REFERENCES

(1) Love, J. C.; Estroff, L. A.; Kriebel, J. K.; Nuzzo, R. G.; Whitesides, G. M. Self-assembled monolayers of thiolates on metals as a form of nanotechnology. *Chem. Rev.* **2005**, *105*, 1103−1169.

(2) Schreiber, F. Structure and growth of self-assembling monolayers. *Prog. Surf. Sci.* **2000**, *65*, 151−256.

(3) Poirier, G. E. Characterization of organosulfur molecular monolayers on Au(111) using scanning tunneling microscopy. *Chem. Rev.* **1997**, *97*, 1117−1127.

(4) Vericat, C.; Vela, M. E.; Benitez, G.; Carro, P.; Salvarezza, R. C. Self-assembled monolayers of thiols and dithiols on gold: new challenges for a well-known system. *Chem. Soc. Rev.* **2010**, *39*, 1805−1834.

(5) Rohwerder, M.; Deweldige, K.; Vago, E.; Viefhaus, H.; Stratmann, M. Adsorption of self-assembled monolayers of mercaptan on gold. *Thin Solid Films* **1995**, *264*, 240−245.

(6) Pale-Grosdemange, C.; Simon, E. S.; Prime, K. L.; Whitesides, G. M. Formation of self-assembled monolayers by chemisorption of

derivatives of oligo(ethylene glycol) of structure HS(CH2)11-(OCH2CH2)mOH on gold. *J. Am. Chem. Soc.* **1991**, *113*, 12−20.
(7) Maoa, C.; Qiua, Y.; Sang, H.; Mei, H.; Zhu, A.; Shen, J. Various approaches to modify biomaterial surfaces for improving hemocompatibility. *Adv. Colloid Interface Sci.* **2004**, *110*, 5−17.
(8) Schierbaum, K. D.; Weiss, T.; Thoden van Velzen, E. U.; Engbersen, J. F. J.; Reinhoudt, D. N.; Göpel, W. Molecular recognition by self-assembled monolayers of cavitand receptors. *Science* **1994**, *265*, 1413−1415.
(9) Anker, J. N.; Hall, W. P.; Lyandres, O.; Shah, N. C.; Zhao, J.; Van Duyne, R. P. Biosensing with plasmonic nanosensors. *Nat. Mater.* **2008**, *7*, 442−453.
(10) Shin, M. J.; Yang, M.; Shin, J. S. Sensing capability of molecularly imprinted self-assembled monolayer using terphenylpropanethiol. *Particul. Sci. Technol.* **2012**, *30*, 543−552.
(11) Finklea, H. O. Electrochemistry of organized monolayers of thiols and related molecules on electrodes. *Electroanal. Chem.* **1996**, *19*, 109−335.
(12) Eckermann, A. L.; Feld, D. J.; Shaw, J. A.; Meade, T. J. Electrochemistry of redox-active self-assembled monolayers. *Coord. Chem. Rev.* **2010**, *254*, 1769−1802.
(13) Huang, C.; Moosmann, M.; Jin, J. H.; Heiler, T.; Walheim, S.; Schimmel, T. Polymer blend lithography: A versatile method to fabricate nanopatterned self-assembled monolayers. *Beilstein J. Nanotechnol.* **2012**, *3*, 620−628.
(14) Xia, Y. N.; Whitesides, G. M. Soft lithography. *Angew. Chem., Int. Ed.* **1998**, *37*, 550−575.
(15) Geyer, W.; Stadler, V.; Eck, W.; Zharnikov, M.; Gölzhäuser, A.; Grunze, M. Electron-induced crosslinking of aromatic self-assembled monolayers: Negative resists for nanolithography. *Appl. Phys. Lett.* **1999**, *75*, 2401−2403.
(16) Zharnikov, M.; Grunze, M. Modification of thiol-derived self-assembling monolayers by electron and x-ray irradiation: Scientific and lithographic aspects. *J. Vac. Sci. Technol. B* **2002**, *20*, 1793−1807.
(17) Song, H.; Reed, M. A.; Lee, T. Single molecule electronic devices. *Adv. Mater.* **2011**, *23*, 1583−1608.
(18) McCreery, R. L.; Bergren, A. J. Progress with molecular electronic junctions: meeting experimental challenges in design and fabrication. *Adv. Mater.* **2009**, *21*, 4303−4322.
(19) Hains, A. W.; Liu, J.; Martinson, A. B. F.; Irwin, M. D.; Marks, T. J. Anode interfacial tuning via electron-blocking/holetransport layers and indium tin oxide surface treatment in bulk-heterojunction organic photovoltaic cells. *Adv. Funct. Mater.* **2010**, *20*, 595−606.
(20) Steim, R.; Kogler, F. R.; Brabec, C. J. Interface materials for organic solar cells. *J. Mater. Chem.* **2010**, *20*, 2499−2512.
(21) Käfer, D.; Bashir, A.; Witte, G. Interplay of anchoring and ordering in aromatic self-assembled monolayers. *J. Phys. Chem. C* **2007**, *111*, 10546−10555.
(22) Tao, F.; Bernasek, S. L. Understanding odd-even effects in organic self-assembled monolayers. *Chem. Rev.* **2007**, *107*, 1408−1453.
(23) Käfer, D.; Witte, G.; Cyganik, P.; Terfort, A.; Wöll, C. A comprehensive study of self-assembled monolayers of anthracenethiol on gold: Solvent effects, structure, and stability. *J. Am. Chem. Soc.* **2006**, *128*, 1723−1732.
(24) Cyganik, P.; Buck, M.; Azzam, W.; Wöll, C. Self-assembled monolayers of ω-biphenylalkanethiols on Au(111): influence of spacer chain on molecular packing. *J. Phys. Chem. B* **2004**, *108*, 4989−4996.
(25) Azzam, W.; Cyganik, P.; Witte, G.; Buck, M.; Wöll, C. Pronounced odd-even changes in the molecular arrangement and packing density of biphenyl-based thiol SAMs: A combined STM and LEED study. *Langmuir* **2003**, *19*, 8262−8270.
(26) Azzam, W.; Fuxen, C.; Birkner, A.; Rong, H.-T.; Buck, M.; Wöll, C. Coexistence of different structural phases in thioaromatic monolayers on Au(111). *Langmuir* **2003**, *19*, 4958−4968.
(27) Leung, T. Y. B.; Schwartz, P.; Scoles, G.; Schreiber, F.; Ulman, A. Structure and growth of 4-methyl-4′-mercaptobiphenyl monolayers on Au(111): a surface diffraction study. *Surf. Sci.* **2000**, *458*, 34−52.
(28) Liu, J. X.; Schüpbach, B.; Bashir, A.; Shekhah, O.; Nefedov, A.; Kind, M.; Terfort, A.; Wöll, C. Structural characterization of self-assembled monolayers of pyridine-terminated thiolates on gold. *Phys. Chem. Chem. Phys.* **2010**, *12*, 4459−4472.
(29) Silien, C.; Buck, M.; Goretzki, G.; Lahaye, D.; Champness, N. R.; Weidner, T.; Zharnikov, M. Self-assembly of a pyridine-terminated thiol monolayer on Au(111). *Langmuir* **2009**, *25*, 959−967.
(30) Mishina, E.; Tamura, T.; Sakaguchi, H.; Kulyuk, L.; Nakabayashi, S. Photoluminescence studies of oligothiophene self-assembled monolayers at low excitation energy. *J. Chem. Phys.* **2004**, *120*, 9763−9768.
(31) Fuxen, C.; Azzam, W.; Arnold, R.; Terfort, A.; Witte, G.; Wöll, C. Structural characterization of organothiolate adlayers on gold: The case of rigid, aromatic backbones. *Langmuir* **2001**, *17*, 3689−3695.
(32) Ishida, T.; Mizutani, W.; Azehara, H.; Miyake, K.; Aya, Y.; Sasaki, S.; Tokumoto, H. Molecular arrangement and electrical conduction of self-assembled monolayers made from terphenyl thiols. *Surf. Sci.* **2002**, *514*, 187−193.
(33) Ishida, T.; Mizutani, W.; Azehara, H.; Sato, F.; Choi, N.; Akiba, U.; Fujihira, M.; Tokumoto, H. Adsorption processes of self-assembled monolayers made from terphenyl thiols. *Langmuir* **2001**, *17*, 7459−7463.
(34) Ishida, T.; Mizutani, W.; Akiba, U.; Umemura, K.; Inoue, A.; Choi, N.; Fujihira, M.; Tokumoto, H. Lateral electrical conduction in organic monolayer. *J. Phys. Chem. B* **1999**, *103*, 1686−1690.
(35) Ishida, T.; Sano, M.; Fukushima, H.; Ishida, M.; Sasaki, S. Stability of terphenyl self-assembled monolayers exposed under UV irradiation. *Langmuir* **2002**, *18*, 10496−10499.
(36) Ishida, T.; Choi, N.; Mizutani, W.; Tokumoto, H.; Kojima, I.; Azehara, H.; Hokari, H.; Akiba, U.; Fujihira, M. High-resolution X-ray photoelectron spectra of organosulfur monolayers on Au(111): S(2p) spectral dependence on molecular species. *Langmuir* **1999**, *15*, 6799−6806.
(37) Ishida, T.; Fukushima, H.; Mizutani, W.; Miyashita, S.; Ogiso, H.; Ozaki, K.; Tokumoto, H. Annealing effect of self-assembled monolayers generated from terphenyl derivatized thiols on Au(111). *Langmuir* **2002**, *18*, 83−92.
(38) Kang, H.; Shin, D. G.; Han, J. W.; Ito, E.; Hara, M.; Noh, J. Unique ordered domains of biphenylthiol self-assembled monolayers on Au(111). *J. Nanosci. Nanotechnol.* **2012**, *12*, 557−562.
(39) Matei, D. G.; Muzik, H.; Gölzhäuser, A.; Turchanin, A. Structural investigation of 1,1′-biphenyl-4-thiol self-assembled monolayers on Au(111) by scanning tunneling microscopy and low-energy electron diffraction. *Langmuir* **2012**, *28*, 13905−13911.
(40) Duan, L.; Garrett, J. An investigation of rigid p-methylterphenyl thiol self-assembled monolayers on Au(111) using reflection−absorption infrared spectroscopy and scanning tunneling microscopy. *J. Phys. Chem. B* **2001**, *105*, 9812−9816.
(41) Sabatani, E.; Cohne-Boulakia, J.; Bruening, M.; Rubinstein, I. Thioaromatic monolayers on gold: a new family of self-assembling monolayers. *Langmuir* **1993**, *9*, 2974−2981.
(42) Korolkov, V. V.; Allen, S.; Roberts, C. J.; Tendler, S. J. B. High-temperature adsorption of p-terphenylthiol on Au(111) surfaces. *J. Phys. Chem. C* **2011**, *115*, 14899−14906.
(43) Frey, S.; Stadler, V.; Heister, K.; Eck, W.; Zharnikov, M.; Grunze, M.; Zeysing, B.; Terfort, A. Structure of thioaromatic self-assembled monolayers on gold and silver. *Langmuir* **2001**, *17*, 2408−2415.
(44) Himmel, H. J.; Terfort, A.; Wöll, C. Fabrication of a carboxyl-terminated organic surface with self-assembly of functionalized terphenylthiols: the importance of hydrogen bond formation. *J. Am. Chem. Soc.* **1998**, *120*, 12069−12074.
(45) Shaporenko, A.; Cyganik, P.; Buck, M.; Terfort, A.; Zharnikov, M. Self-assembled monolayers of aromatic selenolates on noble metal substrates. *J. Phys. Chem. B* **2005**, *109*, 13630−13638.
(46) Bashir, A.; Käfer, D.; Müller, J.; Wöll, C.; Terfort, A.; Witte, G. Selenium as a key element for highly ordered aromatic self-assembled monolayers. *Angew. Chem., Int. Ed.* **2008**, *47*, 5250−5252.
(47) Poirier, G. E. Mechanism of formation of Au vacancy islands in alkanethiol monolayers on Au(111). *Langmuir* **1997**, *13*, 2019−2026.

(48) Harten, U.; Lahee, A. M.; Toennies, J. P.; Wöll, C. Observation of a soliton reconstruction of Au(111) by high-resolution helium-atom diffraction. *Phys. Rev. Lett.* **1985**, *54*, 2619−2622.
(49) Cossaro, A.; Mazzarello, R.; Rousseau, R.; Casalis, L.; Verdini, A.; Kohlmeyer, A.; Floreano, L.; Scandolo, S.; Morgante, A.; Klein, M. L.; Scoles, G. X-ray diffraction and computation yield the structure of alkanethiols on gold(111). *Science* **2008**, *321*, 943−946.
(50) Maksymovych, P.; Sorescu, D. C.; Yates, J. T. Methanethiolate adsorption site on Au(111): A combined STM/DFT study at the single-molecule level. *J. Phys. Chem. B* **2006**, *110*, 21161−21167.
(51) Mamun, A. H. A.; Son, S. B.; Hahn, J. R. Effects of tunneling current on STM imaging mechanism for alkanethiol self-assembled monolayers on Au(111). *Bull. Korean Chem. Soc.* **2011**, *32*, 281−285.
(52) Cyganik, P.; Buck, M.; Wilton-Ely, J. E. D. T.; Wöll, C. Stress in self-assembled monolayers: ω-biphenyl alkane thiols on Au(111). *J. Phys. Chem. B* **2005**, *109*, 10902−10908.
(53) Cyganik, P.; Buck, M.; Strunskus, T.; Shaporenko, A.; Witte, G.; Zharnikov, M.; Wöll, C. Influence of molecular structure on phase transitions: a study of self-assembled monolayers of 2-(aryl)-ethane thiols. *J. Phys. Chem. C* **2007**, *111*, 16909−16919.
(54) Fenter, P.; Eberhardt, A.; Eisenberger, P. Self-assembly of n-alkyl thiols as disulfides on Au(1 1 1). *Science* **1994**, *266*, 1216−1218.
(55) Fenter, P.; Schreiber, F.; Berman, L.; Scoles, G.; Eisenberger, P.; Bedzyk, M. J. On the structure and evolution of the buried S/Au interface in self-assembled monolayers: X-ray standing wave results. *Surf. Sci.* **1998**, *412/413*, 213; Erratum. *Surf. Sci.* **1999**, *425*, 138−139.
(56) Baunach, T.; Ivanova, V.; Scherson, D. A.; Kolb, D. A. Self-assembled monolayers of 4-mercaptopyridine on Au(111): A potential-induced phase transition in sulfuric acid solutions. *Langmuir* **2004**, *20*, 2797−2802.
(57) Zhou, W. P.; Baunach, T.; Ivanova, V.; Kolb, D. M. Structure and electrochemistry of 4,4′-dithiodipyridine self-assembled monolayers in comparison with 4-mercaptopyridine self-assembled monolayers on Au(111). *Langmuir* **2004**, *20*, 4590−4595.
(58) Seo, K.; Borguet, E. Potential-induced structural change in a self-assembled monolayer of 4-methylbenzenethiol on Au(111). *J. Phys. Chem. C* **2007**, *111*, 6335−6342.
(59) Torres, E.; Blumenau, A. T.; Biedermann, P. U. Mechanism for phase transitions and vacancy island formation in alkylthiol/Au(111) self-assembled monolayers based on adatom and vacancy-induced reconstructions. *Phys. Rev. B* **2009**, *79*, 075440.
(60) Pensa, E.; Cortes, E.; Corthey, G.; Carro, P.; Vericat, C.; Fonticelli, M. H.; Benitez, G.; Rubert, A. A.; Salvarezza, R. C. The chemistry of the sulfur-gold interface: in search of a unified model. *Acc. Chem. Res.* **2012**, *45*, 1183−1192.